AIAA JOURNAL
Vol. 49, No. 3, March 2011

Flow Characteristics of Synthetic Jet Induced by Plasma Actuator

A. B. Liu,* P. F. Zhang,† B. Yan,‡ C. F. Dai,§ and J. J. Wang¶
Beijing University of Aeronautics and Astronautics, 100191 Beijing, People's Republic of China

DOI: 10.2514/1.J050563

The flowfield induced by a plasma synthetic jet actuator was investigated by solving Reynolds-averaged Navier–Stokes equations, augmented with a phenomenological model representing the plasma-induced body force imparted by a plasma actuator on the fluid. Flow characteristics of an unsteady plasma synthetic jet in quiescent air were presented. The results indicate that the time-averaged flowfield is quite similar to the steady plasma synthetic jet, the traditional blowing synthetic jet, and the plane jet. The time-averaged streamwise velocity is a little smaller than that of the steady case, but the jet half-width is much larger. This makes the volume and momentum flux of an unsteady plasma synthetic jet larger. With unsteady actuation, a plasma synthetic jet does not exhibit the suction effect of the cavity during the second half-period, as does the traditional blowing synthetic jet. The vortex pair, formed from the wall jets that are produced by plasma actuators, has a strong unsteady effect on the plasma synthetic jet close to the wall. In the far field, the vortex pair coalesces and eventually develops to a continuous jet.

Nomenclature

a	=	height of plasma area
b	=	width of plasma area
b_0	=	jet half-width at plasma synthetic jet orifice
D_c	=	ratio of the electrical force to the inertial force
D_0	=	orifice width of plasma synthetic jet actuator
dc	=	duty cycle
E	=	electric intensity
E_0	=	maximum electric intensity in plasma area
e_c	=	electron charge
F	=	plasma-induced body-force magnitude
F_i	=	plasma-induced body force in the ith direction
f	=	pulsation frequency
L	=	nondimensional stroke length
L_0	=	stroke length
q_c	=	charge density
Re_{U_0}	=	Reynolds number based on the averaged blowing velocity and jet width
T	=	pulsation period
T_d	=	actuation time in one period T
U_0	=	blowing mean velocity
V_m	=	maximum voltage between two electrodes
w	=	distance between the outer edges of plasma synthetic jet actuator
α	=	collision efficiency
Δt	=	time when plasma is formed
δ	=	Dirac delta function of space
ϑ	=	frequency of applied ac voltage
ν	=	kinematic viscosity coefficient
ρ	=	air density
ρ_c	=	electron number density

Received 21 March 2010; revision received 26 October 2010; accepted for publication 12 November 2010.

*Graduate Student, Institute of Fluid Mechanics; liuibing@gmail.com.
†Associate Professor, Institute of Fluid Mechanics; Key Laboratory of Fluid Mechanics (Ministry of Education); pfzhang@buaa.edu.cn (Corresponding Author).
‡Graduate Student, Institute of Fluid Mechanics; yabo_001@hotmail.com.
§Graduate Student, Institute of Fluid Mechanics; chenfengdai@gmail.com.
¶Professor, Institute of Fluid Mechanics; Key Laboratory of Fluid Mechanics (Ministry of Education); jjwang@buaa.edu.cn. Member AIAA.

I. Introduction

A SYNTHETIC jet is a zero-net-mass flux jet that transfers linear momentum to the flow system. It is usually produced by a sinusoidal oscillating membrane or piston, which alternatively forces the working fluid through an orifice into the external flow and entrains the fluid back. During the blowing cycle, the ejected fluid separates at the sharp edges of the orifice and rolls up to form a vortex ring or pair. When the membrane begins its suction cycle, the vortex ring or pair is quite far from the orifice and keeps on propagating away, due to self-induction. Hence, the vortex ring or pair will not be entrained to the cavity, but will coalesce to synthesize a jet, with momentum transferred to the embedding fluid [1].

The synthetic jet has a unique feature compared with traditional blowing and suction flow control methods. It requires neither external air supply nor complex piping, which makes it bear many advantages such as reduced size and weight, improved manufacturability, low cost, and increased reliability. Since the 1990s, a lot of work has been done on its flow structures [2–4] and applications [5–7]. Details can be found in review papers of Glezer and Amitay [1] and Zhang et al. [8]. With the development of microelectromechanical systems, synthetic jets will be increasingly attractive in the field of active flow control [9].

Like all other active flow control methods, it is an inherent requirement to increase the efficiency of a synthetic jet actuator for engineering applications. It is said that the worker must sharpen his tools to make the work well done. The efficiency, working frequency range, response ability, power requirement, maintenance, and reliability of the actuator directly influence its development and application levels. Thus, the development of a synthetic jet actuator with quick response, low weight, small bulk, and high reliability is to be solved first for engineering applications. A synthetic jet actuator is usually driven by piezoelectric membrane or piston. The energy output of a piezoelectric membrane-driven actuator is very low, due to the small vibration magnitude of the membrane. In addition, the efficiency of this type of actuator, if not driven in structural resonance frequency or Helmholtz resonance frequency, will deteriorate [10]. On the contrary, an actuator driven by a piston could provide large energy output, but needs gearings to drive the piston to vibrate, and thus the working frequency is relatively low. To improve the synthetic jet actuator's performance, Liang et al. [11] designed an actuator based on ferromagnetic shape-memory-alloy composite and hybrid mechanism, which can produce a synthetic jet of about

190 m/s under an actuation frequency of 220 Hz. General Electric Corporation designed a piezoelectric synthetic jet actuator whose velocity can achieve 250 m/s. It has been applied to control the wake of low-altitude navigation and targeting infrared for a night pod on the F-16 for Mach numbers from 0.4 to 0.85 and altitudes from 5000 to 35,000 ft. The results showed that the intensity of the fluctuating pressures in the wake can be suppressed with the synthetic jet at the trailing edge of the pod. Thus, the actuator attenuated the impact of the wake on an F-16's pelvic fin and avoided its damage [12].

Recently, Jacob et al. [13] proposed a new synthetic jet actuator: the plasma synthetic jet (PSJ) actuator, based on the dielectric barrier discharge (DBD) plasma actuator (i.e., plasma actuator, for brevity in this paper). The PSJ actuator is composed of two plasma actuators, which produce two wall jets moving oppositely. The wall jets encounter in the center of the PSJ actuator and roll up to form a jet normal to the wall (see Fig. 1).

The PSJ actuator not only inherits the advantages of the traditional blowing synthetic jet actuator and plasma actuator, but also precludes almost all the drawbacks that the latter two actuators cannot avoid. For example, the PSJ actuator has no orifice, which gets rid of orifice jam of the traditional blowing synthetic jet actuator [14] and enhances its adaptability to the environment. So it is easy for maintenance. In addition, the PSJ actuator is completely composed of circuit components. Consequently, its efficiency is not affected by structural resonance frequency or Helmholtz resonance frequency, which realizes broad frequency bandwidth and quick response. Compared with a plasma-actuator-produced wall jet, PSJ is normal to the wall, which endows itself with the ability to bring larger-momentum fluid from the main flow to the boundary layer; therefore, it can control the boundary layer with less energy input. But the traditional plasma actuator, which injects momentum directly to the boundary layer and produces a wall-paralleled jet, needs more energy for high-speed flow control.

Santhanakrishnan and Jacob [15–17] investigated the flowfield of the PSJ by wind-tunnel experiments. The results indicated that both velocity profiles of the PSJ and continuous jet satisfy the same self-similarity rule, and the maximum instantaneous jet velocity of an unsteady PSJ was larger than that of the steady PSJ. But these experimental studies only gave the velocity profiles of the PSJ without flow structure details. To investigate the vortex formation and evolution, both the instantaneous and time-averaged flowfields of the PSJ are presented through numerical simulation in this paper. To present more general results, key parameters of the PSJ actuator in this study are transformed to the widely used dimensionless parameters in traditional blowing synthetic jet investigation, and the flow characteristics of these two synthetic jets are compared.

II. Governing Equations and Numerical Method

In the present work, the plasma-induced body force is represented by a phenomenological model proposed by Shyy et al. [18]. This model provides the primary control mechanism introduced by the plasma actuator, which, as described earlier, will yield a wall jet by momentum injection. Shyy et al. [18] validated the model by simulating a DBD plasma-induced wall jet. They found that the velocity profiles at different upstream and downstream locations of the actuator fit quite well with the experimental results. Furthermore, recent computations, which compared the phenomenological model with a first-principles approach, demonstrated that the same qualitative flow control behavior was captured with both methodologies [19]. Zhang et al. [20] also used this model to study a plasma Gurney flap to enhance an airfoil's lift by simulation, and it worked well to present the main influence of the plasma actuator.

In the present study, the flowfield is assumed to be described by the Reynolds-averaged Navier–Stokes (RANS) equations, augmented by source terms representing the local forcing of the DBD device with user-defined functions in FLUENT [21]. For unsteady incompressible flow, the conservation of mass and momentum equations can be written as

$$\frac{\partial u_i}{\partial x_i} = 0 \qquad \frac{\partial u_i}{\partial t} + u_i \frac{\partial u_i}{\partial x_j} = -\frac{1}{\rho}\frac{\partial p}{\partial x_i} - \frac{\partial}{\partial x_j}\left(\nu \frac{\partial u_i}{\partial x_j}\right) + F_i \quad (1)$$

In the momentum equations, F_i is the body force induced by the plasma actuator.

Shyy et al. [18] observed through the experiments that the induction of the plasma actuator only has an effect on the upper surface of the covered electrode. In addition, the electric intensity is strongest in the region closest to the inner edges of the two electrodes and decreases linearly in magnitude as one moves away from this region. These indicate that the probability for plasma formation is greater in the region of stronger electric fields [18]. Based on these observations, Shyy et al. [18] ignored the secondary factors that may influence the plasma formation and assumed that the electrical force of plasma actuator acts only on a triangular region with width b and height a, as shown in Fig. 1. The electrical force distribution is the same as the electric intensity described before. It reaches the minimum value at the hypotenuse of the triangular region. Though ac power is applied to the actuator, the plasma induction to the ambient air is directed from the exposed electrode to the covered electrode. Thus, the electrical force is assumed to be parallel to the hypotenuse of the triangular region and points downstream of each plasma actuator (as shown in Fig. 1). The magnitude of electric intensity at the inner edges of the two electrodes is $E_0 = V_m/d$, where V_m and d are the maximum voltage and the distance between two electrodes, respectively. The electric intensity magnitude in the left triangular region can be written as

$$E(x, y) = E_0 - k_1(y + 0.5w) - k_2 x \quad (2)$$

where $k_1 = (E_0 - E_b)/a$, $k_2 = (E_0 - E_b)/b$, and w is the distance between the outer edges of the two plasma areas induced by the PSJ actuator (as shown in Fig. 1). Similarly, the electric intensity magnitude in the right triangular region can be written as

$$E(x, y) = E_0 + k_1(y - 0.5w) - k_2 x \quad (3)$$

The plasma-induced body-force magnitude is

$$F_i(x, y) = \vartheta \alpha \rho_c e_c \Delta t E_i \delta \quad (4)$$

where ϑ is the frequency of the applied voltage, α is a factor to account for the collision efficiency and is assumed to be one in view of the disparity between the electron and the neutral particle number densities [18], ρ_c is the electron number density, e_c is the charge of the electron, Δt is the time during which the plasma is formed (corresponds to one half-cycle), E_i is the electric field strength in the ith direction, and δ is the Dirac delta function of space. The plasma-induced body force in the ith (1 for x and 2 for y) direction is

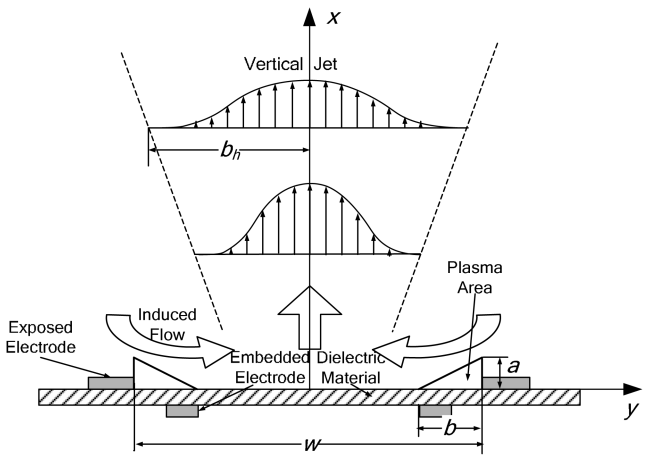

Fig. 1 Sketch of the PSJ actuator and its induced flowfield.

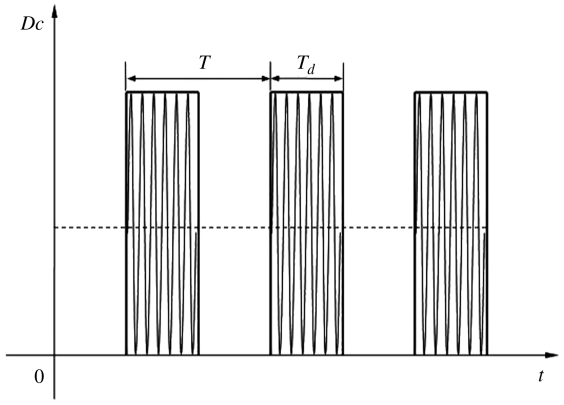

Fig. 2 Signal waveform pattern of the PSJ with unsteady actuation.

$$F_i = \frac{|F|k_i}{\sqrt{k_1^2 + k_2^2}} \tag{5}$$

The previous discussion is the spatial distribution of the body force. The temporal distribution is controlled by the working pattern of the actuation, and a square-wave signal is used to investigate the unsteady actuation (as shown in Fig. 2).

All the computations presented here were carried out using the segregated solver in the FLUENT code to solve the unsteady RANS equations. Pressure implicit with splitting of operators (PISO) is chosen based on a higher degree of approximate relation between the iterative corrections for pressure and velocity. Although the PISO algorithm requires more CPU time, it greatly improves transient calculations, as concluded by Tang and Zhong [22]. The convection and the diffusion terms were discretized using the second-order upwind scheme and the second-order central-differencing scheme, respectively. The discretized algebraic equations were solved using a pointwise Gauss–Seidel iterative algorithm. For this segregated solver, the convergence criterion used was to require the normalized residual to be less than 10^{-5} for the mass and momentum equations. There are 100 time steps in one period and at least 40 iterations in each time step.

The standard k-ω two-equation turbulence model was selected for all the computations of the Navier–Stokes equations. Tang and Zhong [22] pointed out that results from the numerical simulation of the traditional blowing synthetic jet with the standard k-ω turbulent model were closest to the experimental results. Zhang and Wang [3] also used the standard k-ω turbulent model to simulate the synthetic jet in quiescent environment, and the results matched quite well with the benchmark experimental data of NASA Langley Research Center.**

III. Geometry Modeling and Grid Generation

The two-dimensional PSJ actuator composed of two plasma actuators are shown in Fig. 1, in which the right and left triangular regions are the plasma areas of the phenomenological model proposed by Shyy et al. [18]. The width and height of the plasma area are $b = 3$ mm and $a = 1.5$ mm, respectively. The distance between the outer edges of the two plasma areas induced by the PSJ actuator is defined as the actuator's length scale and is denoted by $w = 4b = 12$ mm. As the driving ac frequency of the plasma actuator is so high (of the order of 10^3 Hz), that it is equal to steady actuation. To actuate in an unsteady manner to produce a vortex series of a synthetic jet, a square-wave signal is used, as shown in Fig. 2. A rectangular signal wave pattern is adopted. T_d is the actuation time in one pulsation period T, $f = 1/T = 10$ Hz is the pulsation frequency, and $\mathrm{dc} = T_d/T$ is the duty cycle. To scale the strength of the plasma actuator, a nondimensional parameter D_c is adopted to represent the ratio of the electrical force to the inertial force [23]. It is given by

$$D_c = \frac{q_c E_0 w}{\rho U_{\max}^2} \tag{6}$$

where $q_c = \rho_c . e_c$ is the charge density and E_0 is the maximum electrical intensity in the plasma area. In this study, we adjust D_c to keep the maximum jet velocity in steady actuation to the same as that in Santhanakrishnan and Jacob's experiment [15] and gain $D_c = 8.2$. Because the parameters of the actuator morphology and the power supply in Santhanakrishnan and Jacob's experiment are very commonly used, the actuation strength $D_c = 8.2$ is a usual plasma actuator strength in experiment. To investigate the flow characteristics of an unsteady PSJ, the unsteady actuation strength is $D_c = 16.4$. Considering the duty cycle of an unsteady actuation is $\mathrm{dc} = 0.5$, the energy consumed per period is the same for both actuation methods.

The computational area is rectangular, as shown in Fig. 3, in which the light and dark gray areas at the bottom represent the locations of left and right plasma actuators. The x coordinate is defined as the streamwise direction and the y coordinate is the transverse direction. The coordinate origin is located at the junction point of the PSJ actuator centerline with the wall. The bottom of the computational area is the wall no-slip condition. The right- and left-edge outflow boundaries are $10w$ from the centerline, and the upper-edge outflow boundary is $20w$ from the wall. All the computations are performed using an H-type topological structured-grid system. To capture the vortex-pair formation induced by the PSJ actuator, the grid near the wall and the V geometry area close to the actuator's centerline are refined. Before simulation, three structured 2-D grid systems (i.e., the coarse, medium, and fine cases), with grid points of 300×200, 440×300, and 600×450, respectively, are used to examine the effect of grid resolution. It is observed that the streamwise velocity of the jet centerline calculated with the medium grid and fine grid have almost no difference (about 0.2% deviation), but the velocity with the coarse grid is 3.3% smaller than those with the former two grid systems. Therefore, the medium grid is proper for the present study and is used in the following simulations. The grid dimension of the plasma area is 70×50 [20], and the total node number of the computational area is 134,000.

There are two dimensionless parameters that determine the traditional blowing synthetic jet formation: i.e., the nondimensional stroke length L and the Reynolds number [1]. Two such parameters for the PSJ are calculated for comparison with a traditional blowing synthetic jet. Because PSJ is formed though wall jets produced by the right and left plasma actuators, there is no physical orifice to scale the flowfield. Comparing the time-averaged flowfields of the PSJ with a

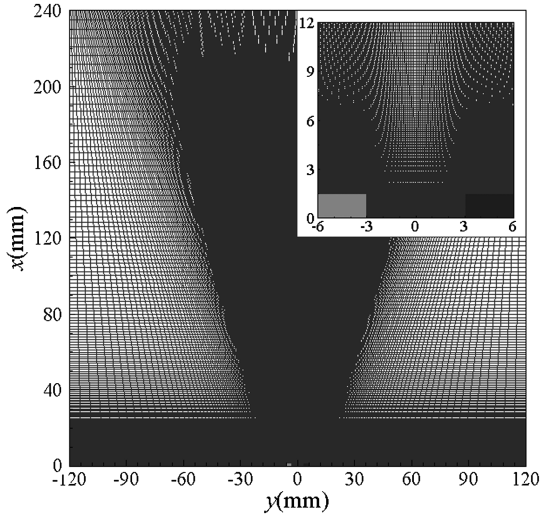

Fig. 3 Computational grid system and its detail distribution in the vicinity of the PSJ actuator.

**Data available online at http://cfdval2004.larc.nasa.gov [retrieved 20 April 2006].

traditional blowing synthetic jet, the width of the PSJ (at the position where the maximum time-averaged streamwise jet velocity exists) is defined as the nominal orifice of the PSJ actuator. All the parameters at this position are denoted by the subscript 0. By this definition, the orifice width D_0 of the PSJ actuator can be expressed as

$$D_0 = 2b_0 \tag{7}$$

where b_0 is the jet half-width. The average velocity at this position is defined as the blowing mean velocity U_0, corresponding to the traditional blowing synthetic jet. To provide a visual reference of b_0, b_h is used to illustrate the half-width of the PSJ at the position with height h in Fig. 1. Since there is no suction stroke for the PSJ actuator, the blowing mean velocity is obtained by temporal and spatial integration of the PSJ streamwise velocity in the whole period, which is different from the treatment for traditional blowing synthetic jet [1,8]. It is defined as

$$U_0 = \frac{1}{T}\int_0^T \bar{u}_0(t)\,\mathrm{d}t \tag{8}$$

Here, $\bar{u}_0(t)$ is the transverse averaged streamwise velocity at the position with maximum streamwise velocity and can be written as

$$\bar{u}_0(t) = \frac{1}{D_0}\int_{-b_0}^{b_0} u_0(y,t)\,\mathrm{d}y \tag{9}$$

D_0 can be calculated at the position $x = 6$ mm with maximum time-averaged streamwise velocity. It can be estimated that the length scale of the PSJ actuator is $D_0 = 2b_0 = 6.24$ mm $\approx 0.5w$, corresponding to the orifice width of the traditional blowing synthetic jet in the following discussions. As a consequence, the averaged blowing jet velocity of the PSJ is $U_0 = 0.281$ m/s; the stroke length $L_0 = U_0T = 28.1$ mm, which yields the nondimensional stroke length $L = U_0T/2b_0 = 4.5$; and the Reynolds number based on the averaged blowing velocity and jet width is $Re_{U_0} = 77.3$.

IV. Results and Discussions

A. Instantaneous Flow Characteristics

Under unsteady actuation, the two wall jets produced by plasma actuators encounter near the center of the PSJ actuator and leave the wall in the vertical direction. Then the two jets merge together to form a vortex pair that moves downstream (positive x direction) by self-induction. Figure 4 shows the contours of instantaneous vorticity in the flowfield of the PSJ at nine different phase angles. In the figure, the dashed lines represent the positive vortex and the solid lines represent the negative vortex. Note that there is only one vortex pair formed in each actuation period, which is similar to the traditional blowing synthetic jet [1]. The difference is that the suction stroke of the traditional blowing synthetic jet will influence the flowfield near the orifice. But the PSJ actuator does not have this defective influence on the ambient flow during the second half-period (corresponding to

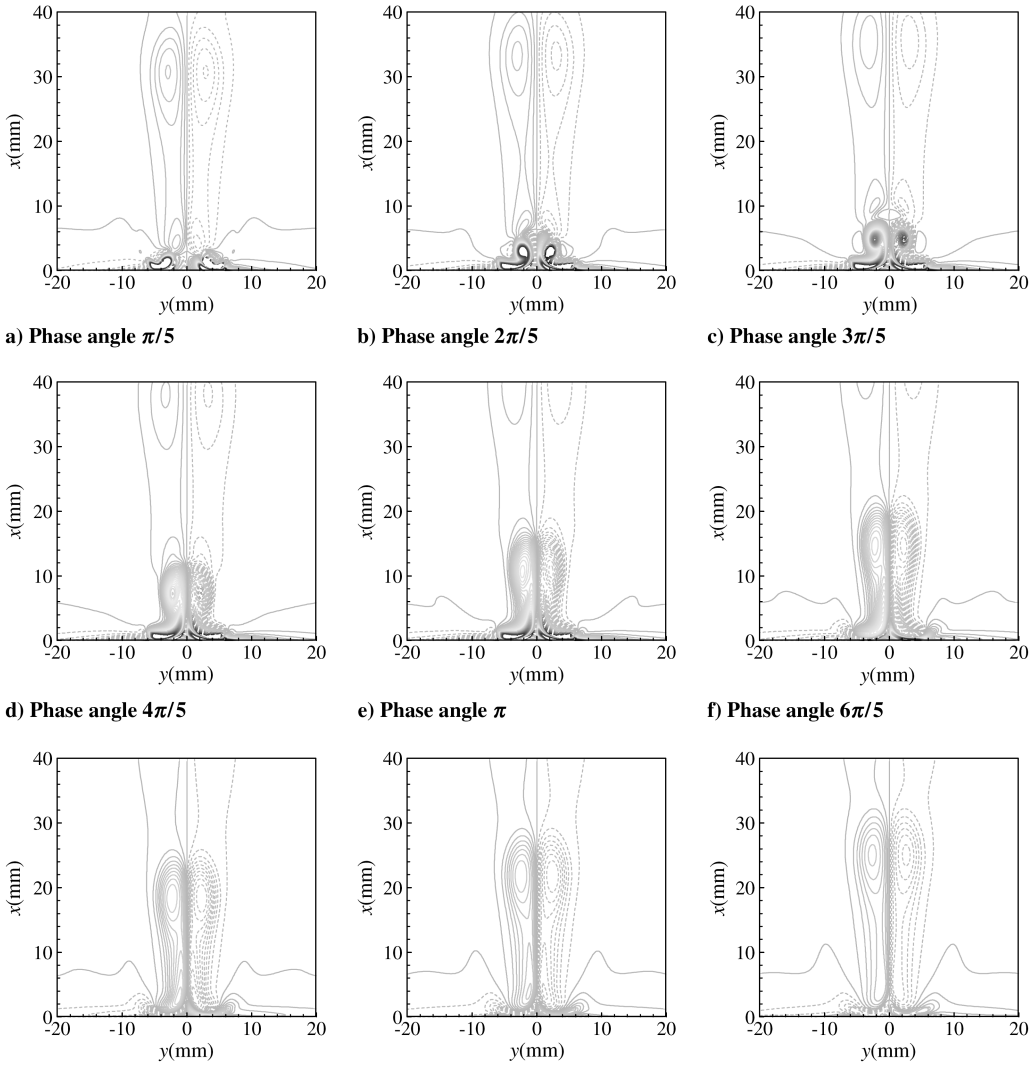

a) Phase angle $\pi/5$ b) Phase angle $2\pi/5$ c) Phase angle $3\pi/5$

d) Phase angle $4\pi/5$ e) Phase angle π f) Phase angle $6\pi/5$

g) Phase angle $7\pi/5$ h) Phase angle $8\pi/5$ i) Phase angle $9\pi/5$

Fig. 4 Vortex-pair formation and convection.

the suction stroke of the traditional blowing synthetic jet), because the body force acting on the neutral air in plasma area will vanish as soon as the PSJ actuator is shut off. To illustrate this phenomenon, the streamlines adjacent to the PSJ actuator at two different phase angles ($4\pi/5$ and $9\pi/5$) are shown in Fig. 5, which presents the flow direction with the PSJ actuator on and off. The figure at phase angle $4\pi/5$ indicates that the fluid near the actuator moves upward, with the wall jets turning to the direction normal to the wall. The other figure at phase angle $9\pi/5$ shows that the flow near the actuator also goes far from the wall in the normal direction, because the vortex pair produced in the first half-period still has self-induction effect, forcing the ambient fluids to move upward. This is different from the traditional blowing synthetic jet's downward movement of the fluid near the actuator [24] in the suction stroke.

In addition to the dominant vortex pair formed during plasma actuation, the trailing vortex (upstream) sheds from the dominant vortex in every actuation period when the actuation is off (Figs. 4f–4i). It is consistent with Zhong et al.'s [25] observations in a traditional blowing synthetic jet that the trailing vortex forms from the dominant vortex. This is because when $L > 4$, and with the circulation of the vortex pair increasing, the vorticity of the main vortex becomes saturated and does not increase any more; thus, the residual circulation will result in trailing vortex in the upstream of the main vortex pair. The actuation strength in the present study is $D_c = 16.4$ for unsteady actuation, and the corresponding non-dimensional stroke length is $L = 4.5$, which is larger than the critical value of $L_{\text{cri}} = 4$ indicated by Zhong et al. [25] for the traditional blowing synthetic jet.

Because the main flow structures of an unsteady PSJ are the vortex pairs produced by plasma actuation, the characteristics of vortex pairs can well reflect the whole flowfield of an unsteady PSJ. The whole flowfield can be obtained by the analysis of the streamwise velocity variation at the centerline of the PSJ actuator. Figure 6 shows the streamwise velocity fluctuations along the centerline in a period at different streamwise positions. As stated above, since there is no suction stroke for the PSJ actuator, its streamwise velocity at the centerline is always positive, as shown in the figure, whereas for a traditional blowing synthetic jet, the streamwise velocity near the actuator is alternatively positive and negative, because of its blowing and suction actuation. It will be positive in the whole period only at the position far enough from the actuator, because the suction effect of the cavity at this position is weaker than the vortex pairs' self-induction effect [26]. This result is the same as that from Santhanakrishnan and Jacob's [15] experimental observations. Though the vortex convection velocity decreases as the vortex pair moves downstream, it is larger than 0.2 m/s in the whole observation window in the present simulation, which indicates continuous momentum output of the PSJ. This is one of the most important characteristics of a synthetic jet [1,8].

To present the instantaneous streamwise velocity distribution along the centerline of the PSJ actuator, Fig. 7 gives the instantaneous streamwise velocity along the centerline at different phase angles.

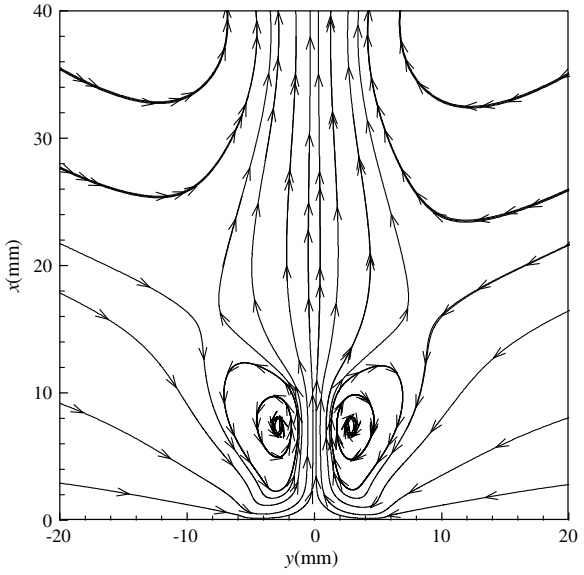

a) 4π/5

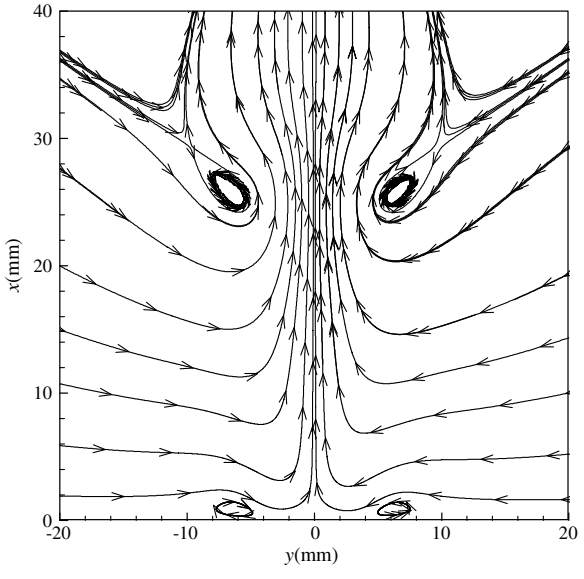

b) 9π/5

Fig. 5 Instantaneous streamlines near the actuator at two different phase angles.

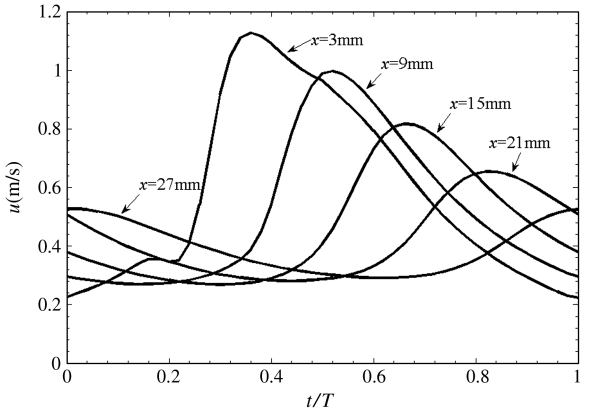

Fig. 6 Streamwise velocity fluctuations in one period at different streamwise positions along the centerline.

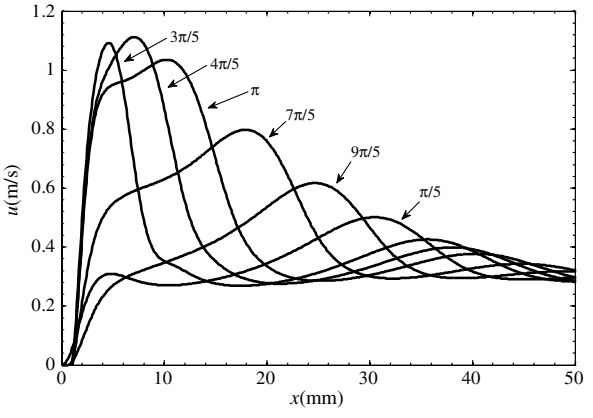

Fig. 7 Instantaneous streamwise velocity distributions along the centerline at different phase angles.

The plasma actuators act from zero phase angle, after which the normal synthetic jet forms. The peak streamwise velocity induced by the vortex pair increases as the duration of actuation time in one pulsation period and achieves the maximum value at phase angle $4\pi/5$. Then the peak streamwise velocity decreases until the end of one pulsation period, because the vortex pair has held enough vorticity, and an increasing amount of ambient fluids are involved into the vortex pair. The amplitude of streamwise velocity along the centerline gets smaller, whereas its influence area becomes larger. After one actuation period, the vortex pair has moved far from the actuator, and the velocity fluctuation amplitude induced by the vortex pair is not as apparent as that in the upstream. Until $x = 50$ mm far from the PSJ actuator, the maximum streamwise velocity of the jet is a little larger than the velocity 0.2 m/s mentioned above, and has no peak value. These results indicate that the vortex structures have gradually merged to a continuous jet.

To show the phenomenon of the vortex pair's merging more directly, Fig. 8 presents the flow structures at zero phase angle over the whole flowfield. It is clear that there exist only two apparent vortex pairs at the streamwise position: $x = 25$ and 50 mm. Beyond this range the vortices has been merged to a jet with continuous momentum output. Santhanakrishnan and Jacob's [15,16] experimental results also show that the vortex forms and develops only in the area near the PSJ actuator and will coalesce in the far field.

Figure 9 presents the PSJ vortex pair's trajectory in space (Fig. 9a) and time (Fig. 9b). The time interval of adjacent sample points in the figures is $T/50$. To show the evolution of the two vortices in a vortex pair, trajectory of the right vortex is shown by mirror reflection about the PSJ actuator centerline. It can be concluded that the vortex pair's initial formation stage is in the region 0 mm $< x <$ 15 mm, in which the vortex pair convects downstream and does not expand in transverse direction. The time scale for this stage corresponds to $t/T = 0 \sim 0.62$ (as shown in Fig. 9b). Then the vortex pair leaves far away from the wall by self-induction, swirls the ambient fluids, and expands in size. The widening of the PSJ is obvious, as shown in Fig. 9a. Beyond $x = 15$ mm, the vortex trajectory expands and the expansion angle remains nearly constant, which is consistent with the linear proportion relation between jet half-width and streamwise position x. This will be discussed in detail in the next section. Figure 9b presents the streamwise position of the vortex pair with time. It shows that the vortex pair's streamwise position increases linearly with time, so the convection velocity of the vortex pair is basically invariable. This feature is different from that of the traditional blowing synthetic jet [2,3], whose convection velocity is influenced by the suction stroke of the cavity.

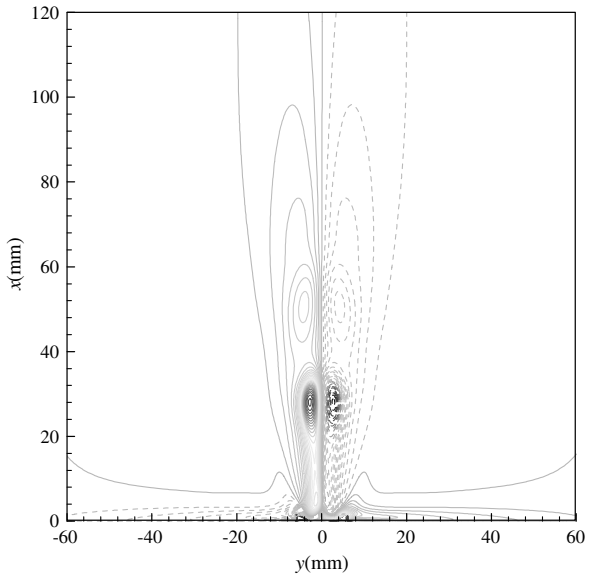

Fig. 8 Instantaneous vorticity contours in the flowfield at zero phase angle.

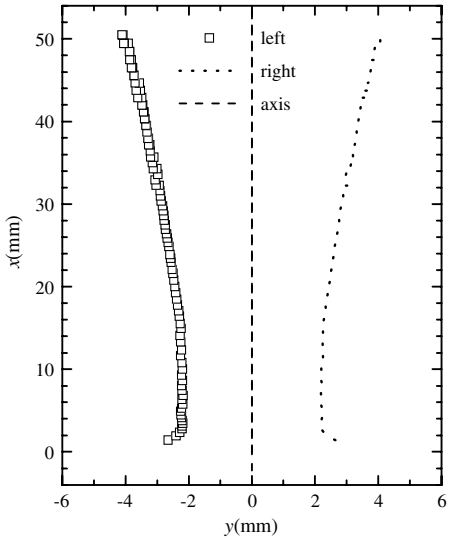

a) Vortex pair's space trajectory

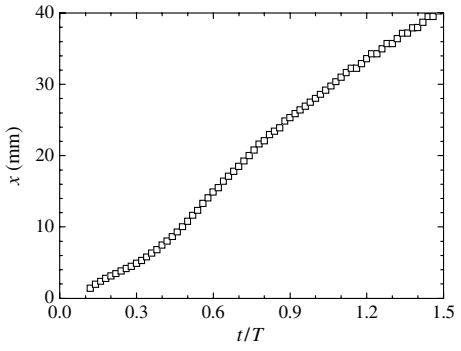

b) Streamwise position of vortex pair vs time

Fig. 9 Vortex-pair trajectories of the PSJ in space and time dimensions.

B. Time-Averaged Flow Characteristics

In this section, the time-averaged flowfield of an unsteady PSJ is presented to investigate the basic feature of the PSJ. As a reference, the flowfield of the steady PSJ with the same actuation strength (i.e., for unsteady actuation $D_c \times \mathrm{dc} = 16.4 \times 0.5 = 8.2$ and for steady actuation $D_c \times \mathrm{dc} = 8.2 \times 1.0 = 8.2$) is also presented. Figure 10 shows the streamwise velocity contours for steady ($w = 4b$ and $D_c = 8.2$) and unsteady ($w = 4b$, $D_c = 16.4$, $\mathrm{dc} = 0.5$, and $f = 10$ Hz) actuated PSJ actuators; these two cases have similar time-averaged velocity distributions. From the figures, it is clear that the jet width of an unsteady actuation is larger than the steady one, which means an unsteady PSJ can involve more ambient fluids into the jet and thus has a higher efficiency for fluid mixing. The time-averaged flowfields of the steady and unsteady PSJs also present the same characteristics as a traditional synthetic jet; i.e., there is a high-velocity core near the centerline of the jet, and the jet velocity decreases downstream, but the jet width increases. It can be estimated from the width of the jet at the initial region that this PSJ corresponds to 6.24 mm orifice width of the traditional blowing synthetic jet.

To quantitatively compare the flowfields of the PSJ with steady and unsteady actuations, figures of velocity profiles, jet width, mass flux, and momentum flux of these two cases will be presented in the following discussions.

Figure 11 gives the time-averaged streamwise velocity profiles at different streamwise positions for steady and unsteady cases. The streamwise velocity has the same profile for both actuation methods, but the magnitude for the steady case is a little larger than that of an unsteady actuation. Near the actuator, the streamwise velocity is negative in both cases (for a line at $x = 3.0$ mm) in the region around $y = \pm 5$ mm, which are just the locations of two plasma actuators. Because the body forces imparted to the fluids by the plasma

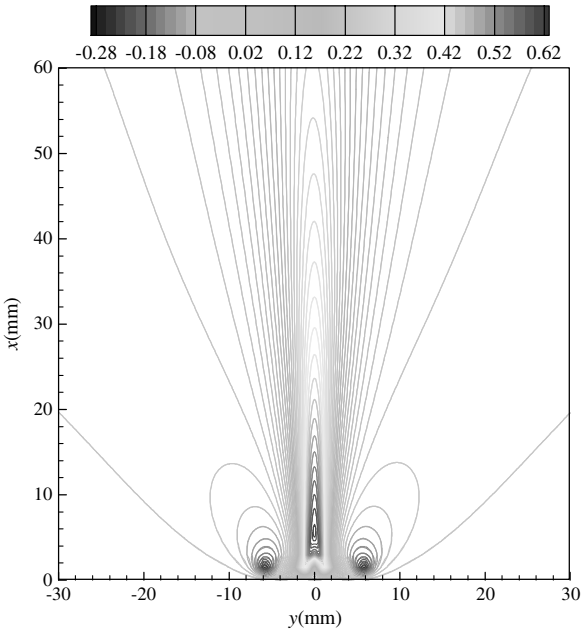

a) Steady actuation

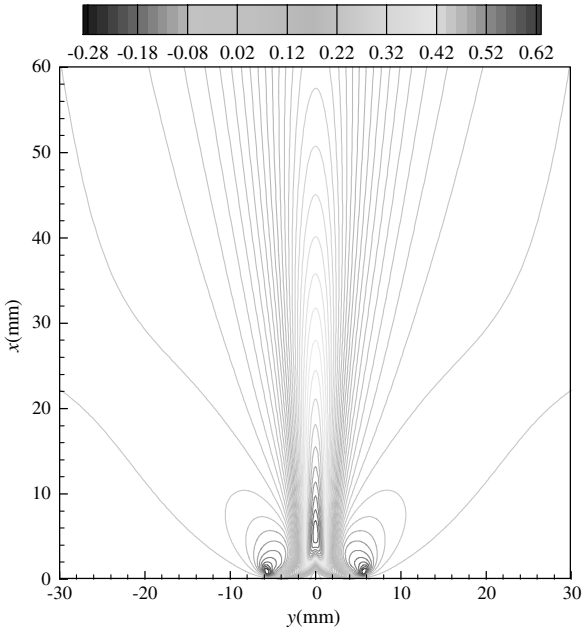

b) Unsteady actuation (time averaged)

Fig. 10 Streamwise velocity contours of the PSJ.

actuators point to the inner sides of the PSJ actuator and face downward, the plasma actuators induce the fluids near this region to flow downward. Far from the actuator downstream, the streamwise velocity is positive because of the induction effect of the vortex pair.

As previously discussed, PSJ is formed as a result of the two impinged wall jets induced by the right and left plasma actuators. Figure 11 shows that the two wall jets have not been merged together at $x = 3$ mm for both steady and unsteady actuations. So there are two peaks on the streamwise velocity profiles (at $x = 3$ mm), which represent the two turned wall jets normal to the wall. Afterward, the two wall jets merge to a unique jet, so there is only one peak for the streamwise velocity profile. The jet velocity reaches the maximum value at $x = 6$ mm. Farther downstream, the jet streamwise velocity decreases, and the jet width increases in sequence.

As the jet develops downstream, its streamwise velocity profiles exhibit the same self-similarity as a traditional blowing synthetic jet (as shown in Fig. 12). In Fig. 12, the streamwise velocity and the

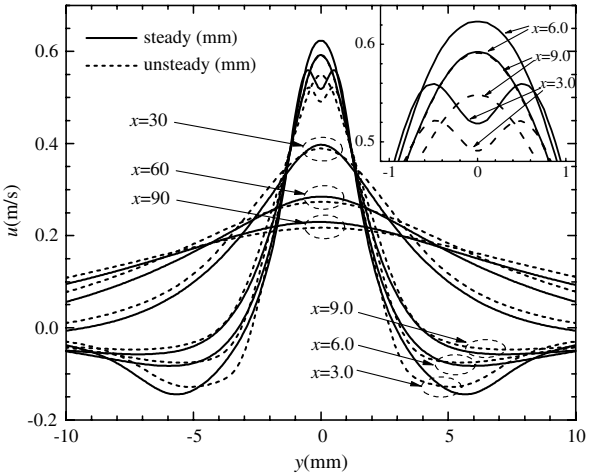

Fig. 11 Streamwise velocity profiles at different streamwise positions of the PSJ with steady/unsteady actuation.

transverse location have been normalized by the maximum time-averaged streamwise velocity and the jet half-width $b_{0.5}$ at each streamwise station (where $b_{0.5}$ is the half-width based on $0.5U_{\text{pp}}$, and U_{pp} is the peak-to-peak streamwise velocity). The streamwise velocity profiles show good self-similarity in the region relatively far from the wall, and the normalized curves match the distribution of hyperbolic cosine function $u/u_{\max} = \cosh^{-2}(A \cdot y/b_{0.5})$ well. Zhang and Wang's [3] numerical simulation and Smith and Glezer's [2] and Smith and Swift's [27] experiments of the traditional blowing

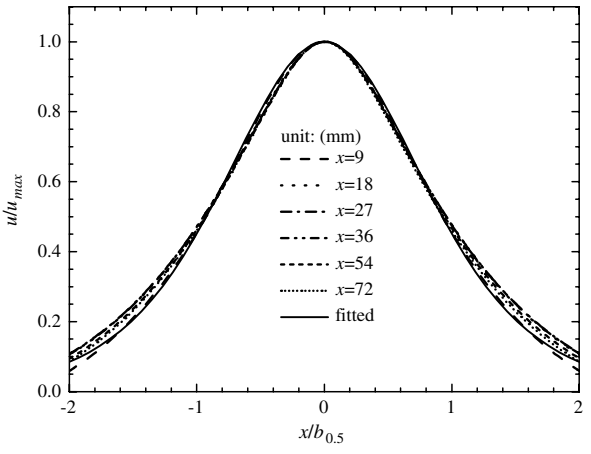

a) Steady actuation

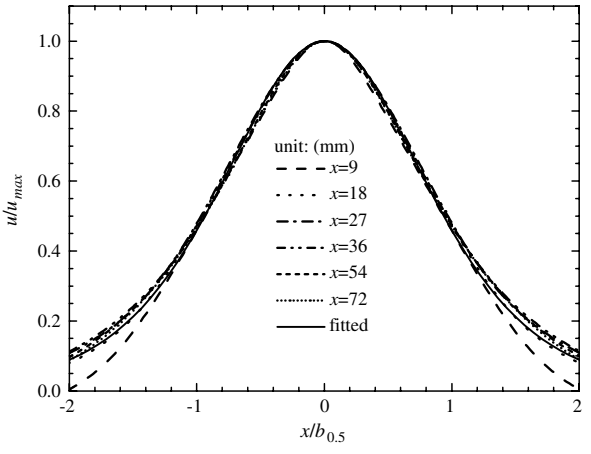

b) Unsteady actuation (time averaged)

Fig. 12 Self-similarity of streamwise velocity profiles.

synthetic jet all show this self-similarity of the streamwise velocity profiles, and it also applies to a plane jet [28]. Thus, it can be concluded that the streamwise velocity of the PSJ, traditional blowing synthetic jet, and plane jet share the same self-similarity profile.

The PSJ is formed by the mergence of two turned wall jets induced by plasma actuators, so the development of wall jets is also very important for the PSJ formation. Figure 13a presents the transverse velocity profiles at several stations near the left plasma actuator. At the stations out of the PSJ actuator ($y = -7.5$ mm, which is just close to the border edge of left plasma actuator), the fluids flow toward the right direction, induced by the plasma actuator. The velocity for both steady and unsteady actuations is very small, and the difference is negligible. When the fluids move into the plasma area, the velocity in the boundary layer increases very quickly under the action of plasma-induced body force, which results in the wall-jet formation. Then the transverse velocity of the wall jet reaches its maximum value (for steady actuation, 0.9 m/s, and for unsteady actuation, 0.75 m/s) at about $y = -4.5$ mm (close to the center of left plasma actuator). Because of the mutual restriction of the two face-to-face wall jets, this position with maximum wall-jet velocity is different from that of a single plasma actuator, whose position is the downstream edge of the plasma actuator [29]. After the two jets encounter, their transverse velocity decreases, and the jets rise up from the wall. Compared with the jet of the steady actuation, the transverse velocity of the wall jet with unsteady actuation is smaller, which could explain the smaller streamwise velocity of the PSJ with unsteady actuation shown in Fig. 11. Combined with the streamwise velocity near the wall, shown in Fig. 13b, it can be concluded that the wall jet started to move away from the wall and turned around to the normal direction at the position between -4.5 mm $< y < -1.5$ mm, which is close to the inner edge of the PSJ actuator.

As shown in Fig. 12, the normalized streamwise velocity profiles of the PSJ fit quite well in the fully developed region. So it is supposed that the streamwise velocity along the centerline and the jet half-width can reflect the jet characteristics as well as that of the traditional blowing synthetic jet [1,2]. Figure 14 gives the streamwise velocity along the centerline of the PSJ actuator. For both steady and unsteady actuations, the jet velocity reaches its maximum at about $x = 6$ mm. Santhanakrishnan and Jacob [17] indicated that the maximum instantaneous velocity of an unsteady actuation was larger than the maximum velocity of the steady actuation. The same conclusion can be reached in the present research. The maximum instantaneous velocity of an unsteady actuation reaches 1.1 m/s (as shown in Fig. 7) and that of the steady actuation is 0.64 m/s (steady actuation results in the equivalent value between the instantaneous velocity and time-averaged velocity, as shown in Fig. 11). This is because the strength of an unsteady actuation is twice that of the steady actuation to ensure the same energy consumption, and thus its energy is more concentrated. Before the streamwise velocity of the PSJ reaches its maximum, it increases very quickly close to the wall because of the turn of the wall jets. Far from this region, the jet streamwise velocity decreases for the vortex entrainment of ambient fluids. The solid line in Fig. 14 is the streamwise velocity decay of the plane jet. It is plotted with the function $u = ax^{-0.5}$. So the decay of streamwise velocity along the centerline for the PSJ and plane jet has a uniform feature, which is the same as Hong's conclusion [5]. Compared with steady actuation, the time-averaged streamwise velocity of the PSJ with unsteady actuation is smaller (refer to Fig. 11). The reason is that unsteady actuation can entrain more surrounding fluid into the jet, and thus the mass flux will be larger than that of the steady actuation.

Smith and Swift [27] showed that the half-width of the traditional blowing synthetic jet increases linearly in the streamwise direction. In addition, the half-width of the plane jet also increases linearly [28]. Figure 15 shows the half-width $b_{0.5}$ of the PSJ with streamwise distance. It can be concluded that the jet half-widths of these three types of jets all increase linearly downstream. But the jet half-width of an unsteady PSJ is larger than that of the steady actuation, which indicates the stronger entrainment of an unsteady PSJ than the steady case. The figure also gives the fitted straight lines of the sample data points for both steady and unsteady cases. The expansion angle of the PSJ with unsteady actuation is 6.55°, which is obviously larger than the 5.41° of the steady case. The fitted lines are prolonged to intersect with the transverse axis, on which the PSJ actuator lies, to estimate the virtual source of the PSJ. By this treatment, it shows that the virtual sources of unsteady and steady cases are $x = -3$ and -5.5 mm, respectively. It means that the virtual source of the PSJ is embedded into the wall, which is similar to that of the plane jet [28].

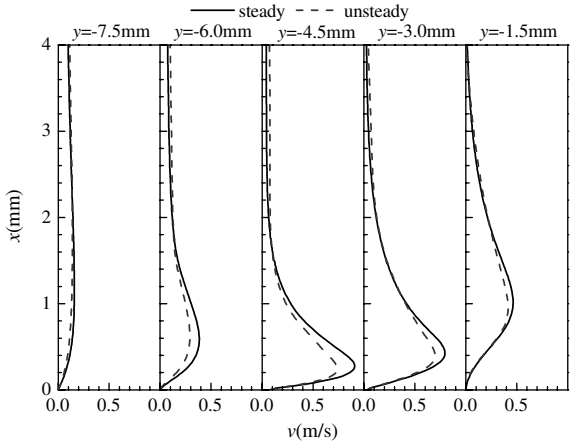

a) Transverse velocity profiles

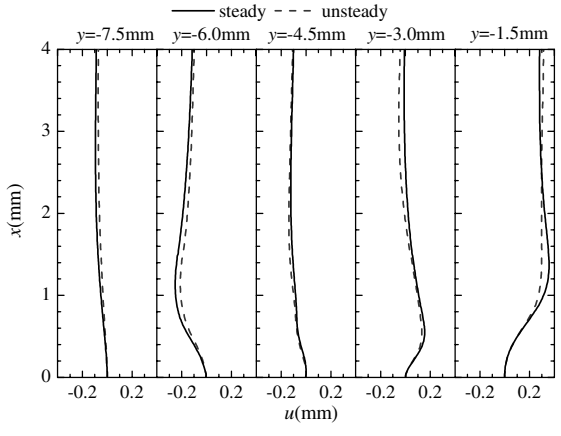

b) Streamwise velocity profiles

Fig. 13 Velocity profiles of the steady/unsteady actuation near the left actuator.

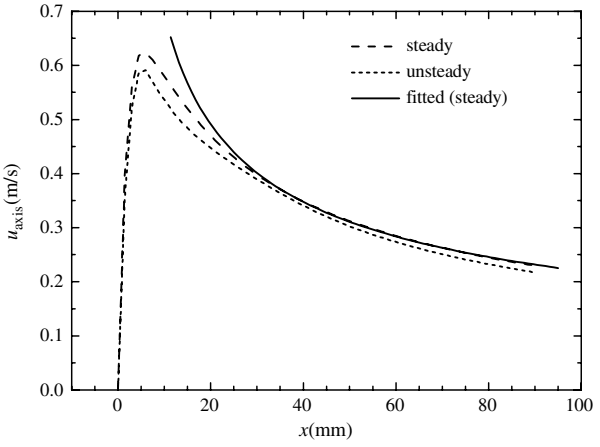

Fig. 14 Streamwise velocity distributions on the centerline of the PSJ actuator with steady/unsteady actuation.

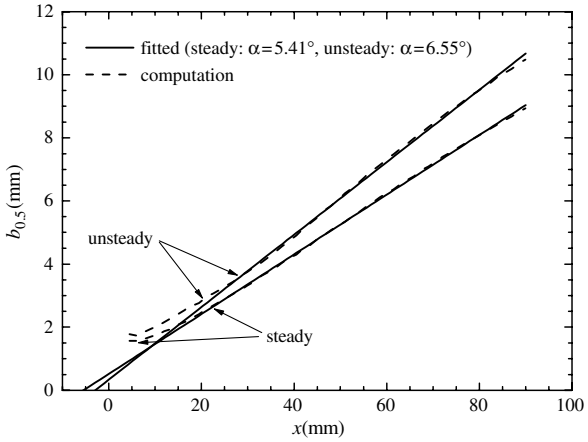

Fig. 15 Jet half-width of the PSJ with steady/unsteady actuation.

To study the features of mass and momentum transportation of the PSJ, the volume and momentum flux of the PSJ are calculated by integration of velocity profiles at each streamwise position:

$$Q = \int_{-b_0}^{b_0} u \, \mathrm{d}y \tag{10}$$

$$M = \rho \int_{-b_0}^{b_0} u^2 \, \mathrm{d}y \tag{11}$$

Figures 16 and 17 show the volume and momentum fluxes of the PSJ with streamwise distance. It is clear that the volume flux increases very quickly close to the wall, which is caused by the direction change of the wall jets. Then the volume flux far downstream exhibits parabolic distribution. This result is the same as that of the plane jet (whose theoretical distribution is $Q = b + cx^{0.5}$). From the analysis above, though the jet time-averaged streamwise velocity for the steady case is larger (Fig. 11), the jet half-width of an unsteady PSJ is larger than that of the steady case (as shown in Fig. 15). So the volume flux of an unsteady PSJ is larger than that of the steady case. This means that the unsteady PSJ can entrain more ambient fluids into the jet and can achieve a better fluid-mixing effect with the same energy consumption. The momentum flux shown in Fig. 17 also has a similar trend. Near the actuator, the momentum flux increases very quickly as a result of the wall jet's turning. But in the fully developed region, the momentum flux decreases gradually, due to viscous effect. Nevertheless, the momentum flux of an unsteady PSJ is larger than that of the steady case in the fully developed region ($x \geq 15$ mm), which again supports the conclusion that the unsteady PSJ has better flow control ability for fluid mixing, mass transportation, and heat convection.

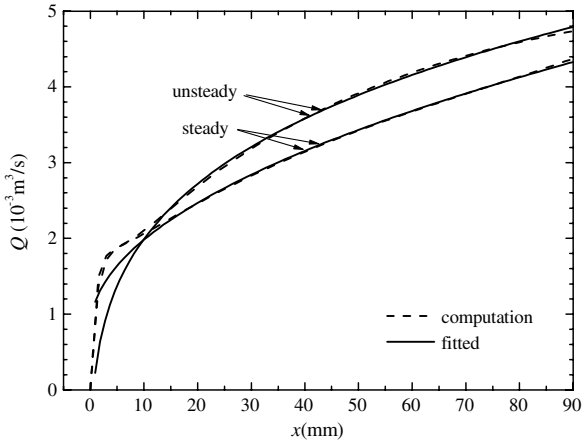

Fig. 16 Volume flux of the PSJ with steady/unsteady actuation.

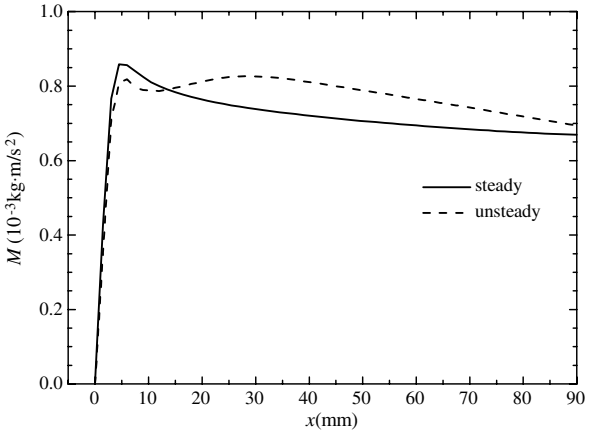

Fig. 17 Momentum flux of the PSJ with steady/unsteady actuation.

V. Conclusions

The PSJ was investigated numerically by solving the Reynolds-averaged Navier–Stokes equations, augmented with a phenomenological model representing the plasma-induced body force imparted by the plasma actuator on the fluid. The instantaneous and time-averaged flowfields of an unsteady PSJ were presented. The main conclusions can be drawn as follows:

1) The time-averaged flowfield of an unsteady PSJ is quite similar to that of the steady case, even to the traditional blowing synthetic jet and plane jet, which includes self-similarity of streamwise velocity profiles, decay of streamwise velocity, expansion of jet width, and variation of mass/momentum fluxes. Although the time-averaged streamwise velocity of an unsteady PSJ is a little smaller than that of the steady case, the jet half-width with unsteady actuation is much larger, which makes its volume flux and momentum flux larger. This indicates that the unsteady PSJ can entrain more ambient fluids into the jet, which is beneficial for mixing of fluid, transportation of mass, and heat.

2) With unsteady actuation, PSJ does not bear the suction effect of the cavity during the second half-period like the traditional blowing synthetic jet. The vortex pair formed from the encountered wall jets has a strong unsteady effect on the PSJ in the region close to the wall (within about 50 mm), which is the same as that of the traditional blowing synthetic jet. In the far field, the vortex pair merges together, and the jet eventually develops to a continuous jet.

Acknowledgments

The present research was supported by the National Natural Science Foundation of China under grant no. 10872021 and the Fundamental Research Funds for the Central Universities under grant no. YWF-10-01-A05.

References

[1] Glezer, A., and Amitay, M., "Synthetic Jets," *Annual Review of Fluid Mechanics*, Vol. 34, 2002, pp. 503–529. doi:10.1146/annurev.fluid.34.090501.094913

[2] Smith, B. L., and Glezer, A., "The Formation and Evolution of Synthetic Jets," *Physics of Fluids*, Vol. 10, No. 9, 1998, pp. 2281–2297. doi:10.1063/1.869828

[3] Zhang, P. F., and Wang, J. J., "Novel Signal Wave Pattern for Efficient Synthetic Jet Generation," *AIAA Journal*, Vol. 45, No. 5, 2007, pp. 1058–1065. doi:10.2514/1.25445

[4] Shan, R. Q., and Wang, J. J., "Experimental Studies of the Influence of Parameters on Axisymmetric Synthetic Jets," *Sensors and Actuators A (Physical)*, Vol. 157, No. 1, 2010, pp. 107–112. doi:10.1016/j.sna.2009.11.006

[5] Hong, G., "Effectiveness of Micro Synthetic Jet Actuator Enhanced by Flow Instability in Controlling Laminar Separation Caused by Adverse Pressure Gradient," *Sensors and Actuators A (Physical)*, Vol. 132, 2006, pp. 607–615. doi:10.1016/j.sna.2006.02.040

[6] Wang, J. J., Feng, L. H., and Xu, C. J., "Experimental Investigations on Separation Control and Flow Structure Around a Circular Cylinder with Synthetic Jet," *Science in China Series E, Technological Sciences*, Vol. 50, No. 5, 2007, pp. 550–559. doi:10.1007/s11431-007-0067-4

[7] Kim, S. H., and Kim, C., "Separation Control on NACA23012 Using Synthetic Jet," *Aerospace Science and Technology*, Vol. 13, 2009, pp. 172–182. doi:10.1016/j.ast.2008.11.001

[8] Zhang, P. F., Wang, J. J., and Feng, L. H., "Review on the Zero-Net-Mass-Flux Jet And the Application in Separation Flow Control," *Science in China Series E, Technological Sciences*, Vol. 51, No. 9, 2008, pp. 1315–1344. doi:10.1007/s11431-008-0174-x

[9] Kiddy, J., Chen, P., Niemczuk, J., Niemczuk, J., DeVoe, D., and Kiger, K., "Active Flow Control Using Micro Electro-Mechanical Systems," AIAA Paper 2000-1561, 2000.

[10] Chaudhari, M., Verma, G., Puranik, B., and Agrawal, A., "Frequency Response of a Synthetic Jet Cavity," *Experimental Thermal and Fluid Science*, Vol. 33, 2009, pp. 439–448. doi:10.1016/j.expthermflusci.2008.10.008

[11] Liang, Y. C., Kuga, Y., and Taya, M., "Design of Membrane Actuator Based on Ferromagnetic Shape Memory Alloy Composite for Synthetic Jet Applications," *Sensors and Actuators A (Physical)*, Vol. 125, 2006, pp. 512–518. doi:10.1016/j.sna.2005.09.002

[12] Shaw, L., Smith, B. L., and Saddoughi, S., "Full Scale Flight Demonstration of Active Flow Control of a Pod Wake," AIAA Paper 2006-3185, 2006.

[13] Jacob, J. D., Ramakumar, K., Anthony, R., and Rivir, R. B., "Control of Laminar and Turbulent Shear Flows Using Plasma Actuators," *4th International Symposium on Turbulence and Shear Flow Phenomena*, Williamsburg, VA, June 2005.

[14] Wu, K. E., and Breuer, K. S., "Dynamics of Synthetic Jet Actuator Arrays for Flow Control," AIAA Paper 2003-4257, 2003.

[15] Santhanakrishnan, A., and Jacob, J. D., "On Plasma Synthetic Jet Actuators," AIAA Paper 2006–317, 2006.

[16] Santhanakrishnan, A., and Jacob, J. D., "Effect of Plasma Morphology on Flow Control Using Plasma Synthetic Jet Actuators," AIAA Paper 2007-783, 2007.

[17] Santhanakrishnan, A., and Jacob, J. D., "Formation and Scaling of Plasma Synthetic Jet Actuators," AIAA Paper 2007-940, 2007.

[18] Shyy, W., Jayaraman, B., and Anderson, A., "Modeling of Glow Discharge-Induced Fluid Dynamics," *Journal of Applied Physics*, Vol. 92, No. 11, 2002, pp. 6434–6443. doi:10.1063/1.1515103

[19] Gaitonde, D. V., Visbal, M. R., and Roy, S., "A Coupled Approach for Plasma-Based Flow Control Simulations of Wing Sections," AIAA Paper 2006-1205, 2006.

[20] Zhang, P. F., Liu, A. B., and Wang, J. J., "Aerodynamic Modification of NACA0012 Airfoil by Trailing Edge Plasma Gurney Flap," *AIAA Journal*, Vol. 47, No. 10, 2009, pp. 2467–2474. doi:10.2514/1.43379

[21] "Fluent 6.3 User's Guide," Ver. 6.3.26, Fluent Inc., Lebanon, NH, 2006.

[22] Tang, H., and Zhong, S., "Two-Dimensional Numerical Study of Circular Synthetic Jets in Quiescent Flows," *The Aeronautical Journal*, Vol. 109, No. 1092, 2005, pp. 89–97. doi:10.2514/1.15633

[23] Gaitonde, D. V., Visbal, M. R., and Roy, S., "Control of Flow Past a Wing Section with Plasma-Based Body Forces," AIAA Paper 2005-5302, 2005.

[24] Utturkar, Y., Holman, R., and Mittal, R., "A Jet Formation Criterion for Synthetic Jet Actuator," AIAA Paper 2003-0636, 2003.

[25] Zhong, S., Jabbal, M., Tang, H., Garcillan, L., Guo, F., Wood, N., and Warsop, C., "Toward the Design of Synthetic Jet Actuators for Full Scale Flight Conditions," *Flow, Turbulence and Combustion*, Vol. 78, 2007, pp. 283–307. doi:10.1007/s10494-006-9064-0

[26] Smith, B. L., and Swift, G. W., "Synthetic Jets at Large Reynolds Number and Comparison to Continuous Jets," AIAA Paper 2001-3030, 2001.

[27] Smith, B. L., and Swift, G. W., "Comparison Between Synthetic Jets and Continuous Jets," *Experiments in Fluids*, Vol. 34, No. 4, 2003, pp. 467–472.

[28] Bickley, W., "The Plane Jet," *Philosophical Magazine*, Ser. 7, Vol. 23, No. 156, 1939, pp. 727–731.

[29] Magnier, P., Boucinha, V., Dong, B. J., Weber, R., Chesneau, A. L., and Hong, D., "Experimental Study of the Flow Induced by a Sinusoidal Dielectric Barrier Discharge Actuator and Its Effects on a Flat Plate Natural Boundary Layer," *Journal of Fluids Engineering*, Vol. 131, No. 1, 2009, Paper 011203. doi:10.1115/1.3026722

W. Anderson
Associate Editor